Dual-polarization silicon nitride Bragg filters with low thermal sensitivity

Elena Duran-Valdeiglesias, Sylvain Guerber, Dorian Oser, Xavier Le Roux, Daniel Benedikovic, Diego Perez-Galacho, Nathalie Vulliet, Sébastien Cremer, Stéphane Monfray, Eric Cassan, et al.

Dual-polarization silicon nitride Bragg filters with low thermal sensitivity

ELENA DURÁN-VALDEIGLESIAS[1], SYLVAIN GUERBER[1,2], DORIAN OSER[1], XAVIER LE ROUX[1], DANIEL BENEDIKOVIC[1], DIEGO PÉREZ-GALACHO[1,3], NATHALIE VULLIET[2], SÉBASTIEN CREMER[2], STEPHANE MONFRAY[2], ERIC CASSAN[1], DELPHINE MARRIS-MORINI[1], CHARLES BAUDOT[2], FRÉDÉRIC BOEUF[2], LAURENT VIVIEN[1], AND CARLOS ALONSO-RAMOS[1,*]

[1] *Centre de Nanosciences et de Nanotechnologies, CNRS, Université Paris-Sud, Université Paris-Saclay, 91120 Palaiseau France*
[2] *STMicroelectronics SAS –850 rue Jean Monnet –38920 Crolles France*
[3] *ITEAM research institute, Universitat Politécnica de Valencia, Camino de Vera s/n, 46022, Valencia, Spain*
[*] *Corresponding author: carlos.ramos@u-psud.fr*

Compiled August 26, 2019

Wideband and polarization independent wavelength filters with low sensitivity to temperature variations have a great potential for wavelength division multiplexing applications. However, simultaneously achieving these metrics is challenging for the silicon-on-insulator photonics technology. Here, we harness the reduced index contrast and the low thermo-optic coefficient of silicon nitride to demonstrate waveguide Bragg grating filters with wideband apolar rejection and low thermal sensitivity. Filter birefringence is reduced by judicious design of a triangularly-shaped lateral corrugation. Based on this approach, we demonstrated silicon nitride Bragg filters with a measured polarization-independent 40 dB optical rejection with negligible off-band excess loss, and a sensitivity to thermal variations below 20 pm/°C.

OCIS codes: (130.3120) Integrated optics devices; (230.7390) Waveguides, planar; (230.1480) Bragg reflector; (040.6040) Silicon.

http://dx.doi.org/10.1364/ao.XX.XXXXXX

Coarse wavelength division multiplexing (CWDM) in the original telecommunications band (O-band), centered around 1.31 μm wavelength, is being extensively developed for optical communication systems targeting data center applications [1]. On the other hand, polarization multiplexing has been identified as a promising approach to further extend the available data capacity [2]. Hence, wideband and polarization independent photonic components are of paramount importance for the development of next generation on-chip datacom systems. Owing to its compatibility with industrial micro-electronic fabrication infrastructures, silicon photonics has a great potential for the implementation of high performance and low-cost opto-electronic circuits. However, Si photonics faces some major challenges, primarily arising from the high-index contrast of the silicon-on-insulator (SOI) technology. Specifically, the performance of SOI devices is typically constrained by stringent fabrication tolerances, high thermal sensitivity and strong polarization dependence. Then, other materials emerged to overcome Si limitations. It is the case of silicon nitride, which is a CMOS-compatible material with a substantially lower thermo-optic coefficient, and reduced index contrast that can be harnessed to substantially relax both, thermal and fabrication constraints. Moreover, the lower birefringence of silicon nitride waveguides opens new opportunities to implement of dual-polarization photonic circuits [3]. Indeed, different efforts are devoted to the development of silicon-nitride-based photonic circuits for datacom applications [4–7].

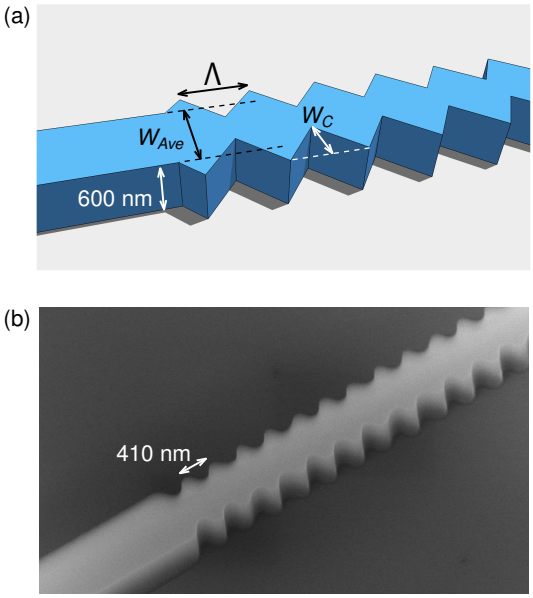

Fig. 1. Proposed silicon nitride Bragg grating filter with triangular corrugation: (a) device schematic and (b) scanning electron microscope image of fabricated filter.

Waveguide Bragg gratings are a key building block in opti-

cal communication systems based on wavelength multiplexing, allowing the implementation of spectral filters [8, 9] and advanced techniques for chip-scale dispersion engineering [10]. To date, most silicon Bragg filters exhibit a strong polarization dependence and temperature sensitivity, both limiting their potential use in CDWM applications. Polarization-independent waveguide Bragg gratings have been implemented in silicon. Proposed devices exploit low-birefringence rib waveguides [11] or the combination of different corrugations at the side and surface of the waveguides [12]. Still, these solutions do not address the thermal sensitivity limitation in silicon. On the other hand, theoretical studies suggest that birefringence compensation and mode degeneracy in silicon nitride Bragg gratings could allow the realization of polarization-independent filters [13], while leveraging the low thermal coefficient in silicon nitride.

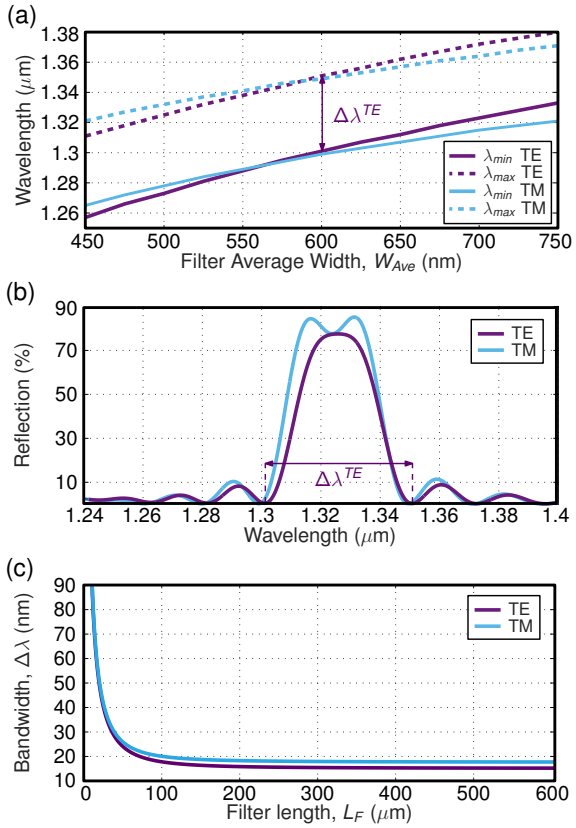

Fig. 2. (a) Calculated maximum and minimum wavelengths of the Bragg reflection as a function of the grating average width (W_{Ave}). (b) Calculated reflection spectra for TE and TM polarizations, considering W_{Ave} = 600 nm. In all cases the silicon nitride thickness is 600 nm, the period is Λ = 410 nm, the corrugation width is W_C = 200 nm, and the filter length is 20 μm. (c) Estimated bandwidth for a triangular filter with W_C = 200 nm as a function of its length, L_F.

Here, we propose to reduce the filter birefringence by implementing silicon nitride Bragg gratings with a triangularly-shaped lateral corrugation (see Fig. 1), designed to yield a quasi-square transversal geometry, where the average waveguide width virtually matches the waveguide thickness. The proposed geometry exhibits almost identical Bragg central wavelength and bandwidth for both, transverse-electric (TE) and transverse-magnetic (TM), polarizations. Capitalizing on this low-birefringence geometry, we experimentally demonstrated silicon nitride Bragg gratings with polarization-agnostic rejection of 40 dB within a 15 nm bandwidth in the O-band. We also show that owing to the reduced thermo-optic coefficient of silicon nitride, these filters exhibit a thermal drift of the Bragg notch wavelength lower than 20 pm/°C. The filters have been fabricated using 248-nm deep-ultraviolet (deep-UV) photolithography in 300 mm Si wafers, showing the compatibility with large-volume fabrication processes.

Bragg gratings reflect the incoming light by exploiting constructive interference of partial back-reflections in a periodic perturbation. Such constructive interference occurs at the Bragg resonance wavelength, that can be calculated as:

$$\lambda_o^{TE/TM} = \frac{n_B^{TE/TM}\Lambda}{p}, \tag{1}$$

where the superscript denotes TE or TM polarization, $\lambda_o^{TE/TM}$ is the central Bragg wavelength, $n_B^{TE/TM}$ is the effective index of the Bloch-Floquet mode that propagates along the periodic waveguide, Λ is the grating period and p (natural number) is the Bragg order. On the other hand, from the coupled-mode theory [14], the bandwidth ($\Delta\lambda^{TE/TM}$) and reflection level ($R^{TE/TM}$) of the Bragg grating can be estimated as:

$$\Delta\lambda^{TE/TM} = \frac{(\lambda_o^{TE/TM})^2}{\pi n_g^{TE/TM}}\sqrt{(\kappa^{TE/TM})^2 + \frac{\pi^2}{L_F^2}}, \tag{2}$$

$$R^{TE/TM} = \tanh^2(\kappa^{TE/TM} L_F), \tag{3}$$

being L_F the filter length, $n_g^{TE/TM}$ the group index and $\kappa^{TE/TM}$ the coupling coefficient of the grating. From Eqs. (1), (2) and (3) it is apparent that implementing polarization independent Bragg gratings requires matching of the effective index, group index and coupling coefficient for both TE and TM polarizations.

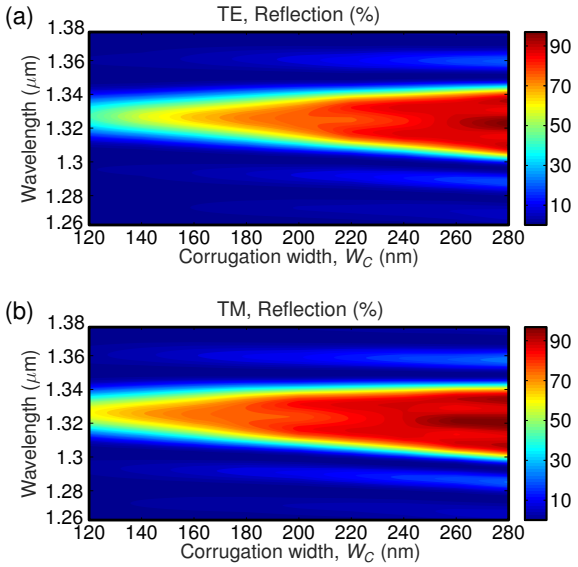

Fig. 3. (a) Calculated reflectivity spectra as a function of the corrugation width, W_C, for (a) TE and (b) TM polarizations considering silicon nitride thickness of 600 nm, W_{Ave} = 600 nm, Λ = 410 nm, and a filter length of 20 μm.

One way to completely suppress the polarization dependence of the filter is to implement a Bragg grating with the same index distribution across the transverse horizontal and vertical axes,

i.e. by realizing an ideal square transversal geometry. However, this would require implementing the same corrugation in the vertical and horizontal walls of the waveguide. Such three-dimensional (3D) corrugation would be challenging to fabricate, compromising the viability of the solution. Here, we propose a comparatively simpler solution that exploits a quasi-square transversal geometry and can be fabricated with a single etch step. The Bragg grating comprises a triangularly-shaped lateral corrugation, as schematically shown in Fig. 1. This grating geometry does not only allow a single-etch process, but also it obviates abrupt index variations that may produce an unwanted excess loss outside the rejection band. The main geometrical parameters that define the grating are: the filter period (Λ), the average waveguide width (W_{Ave}) and the corrugation width (W_C).

For the filter design, we considered a 600 nm-thick silicon nitride guiding layer surrounded by silicon dioxide. We have studied the polarization dependence of the proposed triangularly-shaped SiN Bragg filter by means of 3D finite difference time domain (FDTD) simulations [15]. We considered a corrugation width of W_C = 200 nm, and a pitch of Λ = 410 nm. We have calculated the reflection spectra for a filter length of 20 µm, providing relatively strong reflected signals with a reasonably demanding computation effort. Maximum and minimum Bragg wavelengths, calculated for both TE and TM polarizations as a function of the filter average width, W_{Ave}, are shown in Fig. 2(a). We define the filter bandwidth as the distance between the two nulls delimiting the Bragg reflection band (see, e.g. Fig 2(b)).These two nulls also determine the maximum and minimum wavelengths considered in Fig. 2(a). As shown in Fig. 2(a), both TE and TM polarizations have similar bandwidths in all considered cases, with negligible difference for filter average width near $W_{Ave} = 600$ nm. This region corresponds to a quasi-square filter transversal geometry, where the average grating width approaches the waveguide thickness of 600 nm.

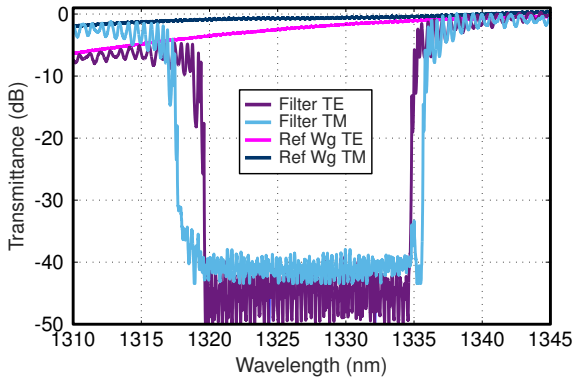

Fig. 4. Transmittance of proposed triangular filter with a length of 500 μm, measured for TE and TM polarizations, compared to reference strip waveguide. The filter has a silicon nitride thickness of 600 nm, period of Λ = 410 nm, W_{Ave} = 600 nm, W_C =200 nm and a filter length of 500 μm.

Typical over- and under-etching fabrication errors mainly change the filter average width, having a weaker effect on the period and corrugation width. Hence, Fig. 2(a) gives an idea of the sensitivity to fabrication errors of the proposed filter. The filter response suffers a wavelength shift of only ~10 nm for waveguide width variations as large as 50 nm. On the other hand, the bandwidth remains almost constant for the average width variations considered here, up to 150 nm. This illustrates the robustness to fabrication errors provided by the lower index contrast of silicon nitride, compared to SOI. Figure 2(b) shows the back-reflections as a function of the wavelength, calculated for TE and TM polarizations considering $W_C = 200$ nm. As a result, both polarizations yield similar calculated bandwidth of ~ 50 nm and reflectivity of ~ 80 %, evidencing the low birefringence of the proposed approach. From the simulated bandwidth and reflectivity, for a corrugation width of W_C = 200 nm and filter length $L_F = 20\,\mu$m, we estimate the filter bandwidth as a function of its length using Eq. (2) [9]. As shown in Fig. 2(c), the bandwidth decreases with the length, reaching a plateau near 15 nm and 17 nm for the TE and TM polarizations, respectively.

We studied the effect of the corrugation width (W_C) for the quasi-square grating configuration, i.e. $W_{Ave} = 600$ nm. The reflection spectra, presented in Fig. 3, are calculated as a function of the corrugation widths. The TM polarization exhibits a slightly wider bandwidth than the TE, with a difference increasing for corrugation widths below $W_C = 200$ nm. Hence, our 3D FDTD calculations predict that quasi-polarization-independent behavior can be achieved just by properly choosing the average width and corrugation width of the triangularly-shaped silicon nitride Bragg grating.

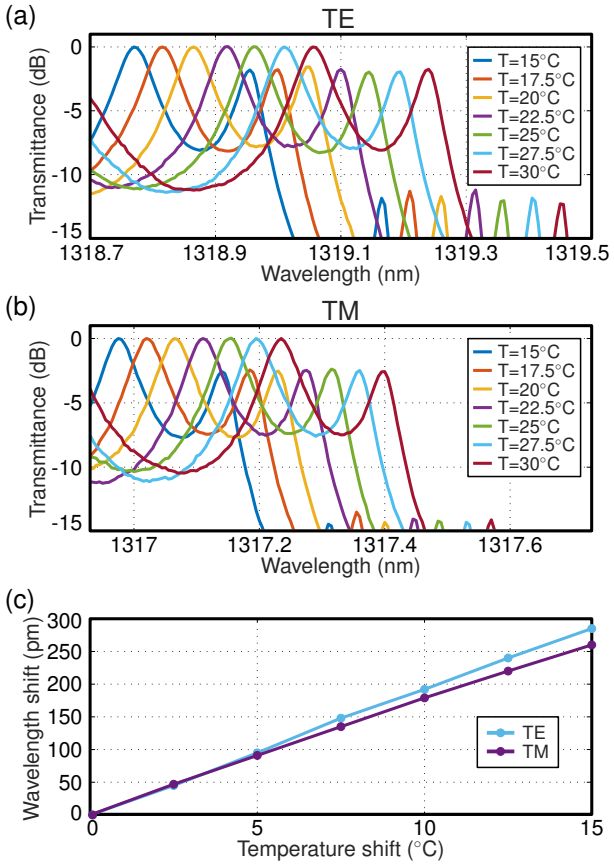

Fig. 5. Measured transmittance of proposed triangular filter at different temperatures for (a) TE and (b) TM polarizations. (c) Wavelength shift as a function of the temperature for both polarizations, extracted from measured spectra.

To experimentally validate the low birefringence of the proposed Bragg grating, we fabricated the filters on the 300 mm silicon photonics R&D platform in ST Crolles (France) [5]. The 600-

nm-thick guiding silicon nitride layer was realized by low temperature plasma enhanced chemical vapor deposition (PECVD). Patterns were defined with 248 nm deep-ultraviolet (deep-UV) photolithography and dry etching. The guiding silicon nitride layer was deposited onto a 1.4 µm-thick buried oxide (BOX) layer, and encapsulated with a 1.5 µm-thick SiO_2 layer. A scanning electron microscope (SEM) image of one of the fabricated filters, taken before encapsulation, is shown in Fig. 1(b). The average waveguide width is reduced by 10 nm approximately.

The optimized waveguide Bragg grating has an average width of W_{Ave} = 600 nm, a corrugation width of W_C =200 nm, and a period of Λ = 410 nm. We chose a corrugation width of W_C =200 nm as a compromise between low birefringence and relaxed minimum feature size. Light is injected/extracted from the chip using fiber-chip grating couplers and cleaved single mode fibers (SMF-28). The fiber-chip couplers have a period of 1 μm and a duty cycle of 50%. They have not been optimized for dual-polarization operation. Thus, they have different insertion loss for TE and TM polarizations. At 1340 nm wavelength, the measured insertion losses for TE and TM are ∼9 dB and ∼16 dB, respectively. Figure 4 shows the measured transmittance spectra of TE and TM polarizations for the same optimized Bragg filter, with a length of 500 µm. As shown in Fig. 2(c), the filter length could be reduced up to 100 μm with a negligible effect on the bandwidth at the cost of a reduced rejection level. For comparison, we also included the TE and TM spectra of a reference strip waveguide with the same length. The measured spectra have been normalized by the insertion loss of the fiber-chip grating couplers at 1340 nm wavelength to remove the effect of polarization-dependent coupling efficiency to the chip. As shown in Fig. 4, the proposed filter yields a remarkably high polarization-independent rejection close to 40 dB in a 15 nm bandwidth. Both, the TE and TM polarizations exhibit almost the same central wavelength, with a bandwidth difference of only 3 nm. In addition, the filter yields negligible off-band excess loss. These experimental results demonstrate the potential of the proposed silicon nitride waveguide Bragg grating for the implementation of polarization-independent high-rejection filters. The ripples in the passband may be reduced by apodizing the corrugation of the filter. This rejection-band filter could be used to implement a pass-band filter by inserting it in the two arms of a Mach-Zehnder interferometer [16].

We have experimentally evaluated temperature-dependent wavelength shift of the filter. The optical characterization was performed using a Peltier system to control the temperature of the filter while monitoring the position of the Bragg resonance. Figures 5(a) and 5(b) show the measured transmittance spectra for both TE and TM polarizations of our 500-μm-long filter. The temperature was varied from 15°C to 30°C, with a step of 2.5°C. We estimate the wavelength dependent shift for TE and TM polarizations by monitoring the edge of the notch band (see Fig. 5(c)). The filter exhibits a nearly linear temperature dependent shift of 19.2 pm/°C for TE and 17.3 pm/°C for TM, respectively. This thermal drift, below 20 pm/°C for both TE and TM polarizations, means a three-fold reduction compared to silicon Bragg gratings [17, 18]. Moreover, we estimated the thermo-optic coefficient of our silicon nitride from the thermal wavelength shift, obtaining a value of $\sim 3.5\times10^{-5}$, comparable to that of recently reported for silicon nitride photonic circuits fabricated with a low-temperature process [4].

In summary, we have proposed and experimentally demonstrated silicon nitride Bragg filters with low thermal sensitivity and dual-polarization operation in the O-band. The proposed filter relies on a triangularly-shaped lateral corrugation that mimics a quasi-square transversal geometry, thereby reducing the Bragg filter birefringence. 3D FDTD simulations show that the polarization dependence of the Bragg resonance wavelength is minimized when the average filter width equals the waveguide thickness, i.e. when a quasi-square transversal geometry is implemented. The filters have been fabricated in the industrial-scale 300 mm silicon photonics R&D platform in ST Crolles. We have experimentally demonstrated a polarization independent Bragg rejection of ∼40 dB, within a bandwidth of 15 nm in the O-band and a negligible off-band excess loss. Experimental characterizations show a thermal drift of the Bragg resonance lower than 20 pm/°C for both polarizations. This is a three-fold reduction compared to standard SOI Bragg grating filters [17, 18]. These results demonstrate the low birefringence and low thermal sensitivity of the proposed filter as well as its compatibility with large-volume fabrication processes, thereby paving the way towards high-performance dual-polarization silicon nitride photonic circuits with a great potential for datacom applications based on CWDM.

FUNDING INFORMATION

European Research Council (ERC POPSTAR) (647342), the European Commission H2020-ICT-27-2017 COSMICC (688516) and the French Industry Ministry Nano2022 project under IPCEI program.

REFERENCES

1. P. Dong, IEEE J. Sel. Top. Quantum Electron., **22**(6), 370 (2016).
2. C. R. Doerr, and T. F. Taunay, IEEE Photon. Technol. Lett., **23**(9), 597 (2011).
3. J. C. Mikkelsen, A. Bois, T. Lordello, D. Mahgerefteh, S. Menezo, and J. K. S. Poon, Opt. Express, **26**(23), 30076 (2018).
4. T. Domínguez Bucio, A. Z. Khokhar, G. Z. Mashanovich, and F. Y. Gardes, Opt. Express, **25**(22), 27310 (2017).
5. S. Guerber, C. Alonso-Ramos, D. Benedikovic, E. Durán-Valdeiglesias, X. Le Roux, N. Vulliet, E. Cassan, D. Marris-Morini, C. Baudot, F. Boeuf, and L. Vivien, IEEE Photon. Technol. Lett., **30**(19), 1679 (2018).
6. J. C. C. Mak, Q. Wilmart, S. Olivier, S. Menezo, and J. K. S. Poon, Opt. Express, **26**(10), 13656 (2018).
7. A. Rahim, E. Ryckeboer, A. Z. Subramanian, S. Clemmen, B. Kuyken, A. Dhakal, A. Raza, A. Hermans, M. Muneeb, S. Dhoore, Y. Li, U. Dave, P. Bienstman, N. Le Thomas, G. Roelkens, D. Van Thourhout, P. Helin, S. Severi, X. Rottenberg, and R. Baets, J. Light. Technol., **35**(4), 639 (2017).
8. J. St-Yves, H. Bahrami, P. Jean, S. LaRochelle, and W. Shi, Opt. Lett., **40**(23), 5471 (2015).
9. D. Oser, D. Pérez-Galacho, C. Alonso-Ramos, X. Le Roux, S. Tanzilli, L. Vivien, L. Labonté, and E. Cassan, Opt. Lett., **43**(14), 3208 (2018).
10. D. T. H. Tan, K. Ikeda, R. E. Saperstein, B. Slutsky, and Y. Fainman, Opt. Lett., **33**(24), 3013 (2008).
11. W. Peng Wong, and K. S. Chiang, J. Light. Technol., **16**(7), 1240 (1998).
12. C. Klitis, G. Cantarella, M. J. Strain, and M, Sorel, Opt. Lett., **42**(15), 3040 (2017).
13. B. Tabti, F. Nabki, and M. Ménard, in Integrated Photonics Research, Silicon and Nanophotonics (OSA, 2017), paper IW2A.5.
14. D. C. Flanders, H. Kogelnik, R. V. Schmidt, and C. V. Shank, Appl. Phys. Lett. **24**(4), 194 (1974).
15. FDTD Solutions, Lumerical Solutions, Inc., http://www.lumerical.com
16. J. Wang, and L. R. Chen, Opt. Express, **23**(20), 26450 (2015).
17. I. Giuntoni, A. Gajda, M. Krause, R. Steingrüber, J. Bruns, and K. Petermann, Opt. Lett., **17**(21), 18518 (2009).
18. N. N. Klimov, S. Mittal, M. Berger, and Z. Ahmed, Opt. Lett., **40**(17), 3934 (2015).

REFERENCES

1. P. Dong, “Silicon Photonic Integrated Circuits for Wavelength-Division Multiplexing Applications,” IEEE J. Sel. Top. Quantum Electron., **22**(6), 370-378 (2016).
2. C. R. Doerr, and T. F. Taunay, “Silicon Photonics Core-, Wavelength-, and Polarization-Diversity Receiver,” IEEE Photon. Technol. Lett., **23**(9), 597-599 (2011).
3. J. C. Mikkelsen, A. Bois, T. Lordello, D. Mahgerefteh, S. Menezo, and J. K. S. Poon, “Polarization-insensitive silicon nitride Mach-Zehnder lattice wavelength demultiplexers for CWDM in the O-band,” Opt. Express, **26**(23), 30076-30084 (2018).
4. T. Domínguez Bucio, A. Z. Khokhar, G. Z. Mashanovich, and F. Y. Gardes, “Athermal silicon nitride angled MMI wavelength division (de)multiplexers for the near-infrared,” Opt. Express, **25**(22), 27310-27320 (2017).
5. S. Guerber, C. Alonso-Ramos, D. Benedikovic, E. Durán-Valdeiglesias, X. Le Roux, N. Vulliet, E. Cassan, D. Marris-Morini, C. Baudot, F. Boeuf, and L. Vivien, “Broadband polarization beam splitter on a silicon nitride platform for o-band operation,” IEEE Photon. Technol. Lett., **30**(19), 1679-1682 (2018).
6. J. C. C. Mak, Q. Wilmart, S. Olivier, S. Menezo, and J. K. S. Poon, “Silicon nitride-on-silicon bi-layer grating couplers designed by a global optimization method,” Opt. Express, **26**(10), 13656-13665 (2018).
7. A. Rahim, E. Ryckeboer, A. Z. Subramanian, S. Clemmen, B. Kuyken, A. Dhakal, A. Raza, A. Hermans, M. Muneeb, S. Dhoore, Y. Li, U. Dave, P. Bienstman, N. Le Thomas, G. Roelkens, D. Van Thourhout, P. Helin, S. Severi, X. Rottenberg, and R. Baets, “Expanding the silicon photonics portfolio with silicon nitride photonic integrated circuits,” J. Light. Technol., **35**(4), 639-649 (2017).
8. J. St-Yves, H. Bahrami, P. Jean, S. LaRochelle, and W. Shi, “Widely bandwidth-tunable silicon filter with an unlimited free-spectral range,” Opt. Lett., **40**(23), 5471-5474 (2015).
9. D. Oser, D. Pérez-Galacho, C. Alonso-Ramos, X. Le Roux, S. Tanzilli, L. Vivien, L. Labonté, and E. Cassan “Subwavelength engineering and asymmetry: two efficient tools for sub-nanometer-bandwidth silicon Bragg filters,” Opt. Lett., **43**(14), 3208-3211 (2018).
10. D. T. H. Tan, K. Ikeda, R. E. Saperstein, B. Slutsky, and Y. Fainman, “Chip-scale dispersion engineering using chirped vertical gratings,” Opt. Lett., **33**(24), 3013-3015 (2008).
11. W. Peng Wong, and K. S. Chiang, “Design of optical strip-loaded waveguides with zero modal birefringence,” J. Light. Technol., **16**(7), 1240-1248 (1998).
12. C. Klitis, G. Cantarella, M. J. Strain, and M. Sorel, “High-Extinction-ratio TE/TM selective Bragg grating filters on silicon-on-insulator,” Opt. Lett., **42**(15), 3040-3040 (2017).
13. B. Tabti, F. Nabki, and M. Ménard, “Polarization insensitive Bragg gratings in Si_3N_4 waveguides,” in Integrated Photonics Research, Silicon and Nanophotonics (OSA, 2017), paper IW2A.5.
14. D. C. Flanders, H. Kogelnik, R. V. Schmidt, and C. V. Shank, “Grating filters for thin-film optical waveguides,” Appl. Phys. Lett. **24**(4), 194–196 (1974).
15. FDTD Solutions, Lumerical Solutions, Inc., http://www.lumerical.com
16. J. Wang, and L. R. Chen, “Low crosstalk Bragg grating/Mach-Zehnder interferometer optical add-drop multiplexer in silicon photonics,” Opt. Express, **23**(20), 26450-26459 (2015).
17. I. Giuntoni, A. Gajda, M. Krause, R. Steingrüber, J. Bruns, and K. Petermann, “Tunable Bragg reflectors on silicon-on-insulator rib waveguides,” Opt. Lett., **17**(21), 18518-18524 (2009).
18. N. N. Klimov, S. Mittal, M. Berger, and Z. Ahmed, “On-chip silicon waveguide Bragg grating photonic temperature sensor,” Opt. Lett., **40**(17), 3934-3936 (2015).